ISSN 0965-5425, Computational Mathematics and Mathematical Physics, 2007, Vol. 47, No. 4, pp. 687–706. © Pleiades Publishing, Ltd., 2007.
Original Russian Text © P.V. Breslavskii, V I. Mazhukin, 2007, published in Zhurnal Vychislitel'noi Matematiki i Matematicheskoi Fiziki, 2007, Vol. 47, No. 4, pp. 717–737.

Dynamically Adapted Grids for Interacting Discontinuous Solutions

P. V. Breslavskii and V. I. Mazhukin

Institute of Mathematical Modeling, Miusskaya pl. 4, Moscow, 125047 Russia

e-mail: immras@orc.ru

Received November 13, 2006

Abstract—Further development of the dynamic adaptation method for gas dynamics problems that describe multiple interactions of shock waves, rarefaction waves, and contact discontinuities is considered. Using the Woodward–Colella problem and a nonuniformly accelerating piston as examples, the efficiency of the proposed method is demonstrated for the gas dynamics problems with shock wave and contact discontinuity tracking. The grid points are distributed under the control of the diffusion approximation. The choice of the diffusion coefficient for obtaining both quasi-uniform and strongly nonuniform grids for each subdomain of the solution is validated. The interaction between discontinuities is resolved using the Riemann problem for an arbitrary discontinuity. Application of the dynamic adaptation method to the Woodward–Colella problem made it possible to obtain a solution on a grid consisting of 420 cells that is almost identical to the solution obtained using the WENO5m method on a grid consisting of 12 800 cells. In the problem for a nonuniformly accelerating piston, a proper choice of the diffusion coefficient in the transformation functions makes it possible to generate strongly nonuniform grids, which are used to simulate the interaction of a series of shock waves using shock wave and contact discontinuity tracking.

DOI: 10.1134/S0965542507040124

Keywords: gas dynamics problems, numerical dynamic grid adaptation method, multiple interaction of discontinuities, contact discontinuities

1. INTRODUCTION

There is rich literature devoted to the generation and adaptation of computational grids [1–7]. By adaptation, we mean the process of grid generation with the optimal distribution of the grid points with respect to the unknown solution. Usually, the generation of optimal grids for a certain problem of mathematical physics is based on a priori information about this solution. However, if no such information is available or if the structure and specific features of the solution are rapidly changing with time, which is characteristic of unsteady problems, then the generation of optimal grids runs into difficulties. An approach to overcome these difficulties is to organize the numerical solution of the problem and grid generation as a unified process. Judging by the number of publications, two approaches to the adaptive grid generation for unsteady problems are presently most popular: adaptive mesh refinement and dynamically adaptive grids.

The adaptive mesh refinement methods [8–10], which have recently received widespread use [11, 12], are used to improve the accuracy of numerical solutions by refining the cells of the grid in the regions where the solution undergoes sharp changes. Refinement can be performed repeatedly, which leads to high-level (from third to sixth level) small cells. The generation of adaptively refined meshes requires complicated algorithms due to a variable number of grid points and the presence of the regions where nonuniformly scaled cells must be matched.

The dynamic adaptation methods [13–21] are less complicated and make it possible to generate grids with a constant [19] or variable [18] number of grid points. In these methods, the control of the distribution of the grid points is achieved by using information about the dynamic behavior of the solution to be found. This makes it possible to concentrate a large number of grid points in the regions where the solution undergoes sharp changes [13]. A close relationship between the dynamic behavior of the solution and the location of the grid points requires that the coordinates of the grid points be recalculated at each time layer. This fact places high requirements upon the consistency of the solution dynamics with the grid points motion. For this reason, the algorithms that do not use any fitting parameters have certain advantages [15]. These features are especially pronounced in the generation of adaptive grids for unsteady gas dynamics problems (see [16–22]), which describe rapidly changing processes. The solution of hyperbolic differential equations,

which governs gas-dynamic processes, imposes additional requirements for the adaptation techniques—these techniques must take into account the discontinuous solutions like shock waves and contact discontinuities.

The existing techniques for solving gas dynamics problems can be divided into two groups: shock capturing methods [23] and explicit front tracking methods [24]. Each of these groups has certain advantages and disadvantages.

The methods for solving hyperbolic systems of equations without discontinuity tracking (the so-called shock capturing methods) have lately been under intensive development. The main problem in designing finite difference schemes in the shock capturing methods is to improve the accuracy of the approximation while ensuring the monotonicity of numerical solutions, which is a nontrivial task in the presence of weak and strong discontinuities. Godunov's theorem (see [25]) claims that, in the linear case, the monotonicity can be ensured only in the first-order schemes. Earlier, artificial viscosity (linear, quadratic, or their combinations) was introduced in the models in order to ensure the monotonicity of solutions. In recent years, artificial viscosity is no longer used due to the development of new methods that smooth discontinuities.

At the early stage, the development of monotone schemes of improved order of accuracy was due to studies [26, 27] and to the flux-corrected transport (FCT) method [28–30]. The next step in the development of difference schemes for hyperbolic equations is the invention of TVD schemes (see, e.g., [31–34]) and of the ENO and WENO methods [35, 36]. Another line of research, which is fairly close to the methods mentioned above, is based on a monotone or quasi-monotone interpolation of grid solutions. The methods based on this technique are known as reconstruction methods. Among them is the so-called piecewise parabolic method (PPM) [37]. A detailed description of the methods mentioned above can be found in book [38] and in survey [39].

The main drawback of all shock capturing methods is the use of a very large number of grid points for achieving the desired accuracy and the necessity to use monotone finite difference schemes. These drawbacks can be significantly mitigated by using controlled grid refinement in the regions where the solution becomes discontinuous.

The use of explicit boundary tracking methods is mainly dictated by some applications, such as energy release or detailed account of the kinetics of various reactions in the discontinuity region. In spite of some difficulties due to the relative complexity of determining the location and time of the appearance of discontinuities and the generation of the grid in regions with variable geometry in multidimensional cases, the discontinuity tracking methods [40–42] have evident advantages for a wide class of problems. In recent years, front tracking methods [40, 43] (they are usually used in combination with adaptive mesh refinement (AMR techniques), gradient adaptation methods based on variational approaches [44] or harmonic mappings [45], and dynamic adaptation methods [4] have been intensively developed.

The purpose of this paper is to further develop the dynamic adaptation method for gas dynamics problems with interacting discontinuous solutions like shock waves, rarefaction waves, and contact discontinuities.

The dynamic adaptation method considered in this paper is based on the transition to an arbitrary time-dependent system of coordinates in which both the grid functions and the coordinates of the grid points are unknown. The transformation of coordinates is performed using the unknown solution; depending on the features of this solution, we obtain one or other distribution of the grid points (see [4, 15, 19, 46]). This approach allows one to use both the shock capturing methods with automatic grid refinement in the vicinity of the solution singularities and the methods based on the explicit tracking of moving boundaries and discontinuities. In [19], both these methods were used to solve the uniformly accelerating piston problem, the efficiency of the algorithms was estimated, and the onset of the self-similar mode was examined.

The features of the dynamic adaptation method will be demonstrated using the Woodward–Colella test problem [37] and the nonuniformly accelerating piston problem; recently, the former problem has become the most widespread problem for testing new numerical methods in gas dynamics.

The main difficulties in the examples considered in this paper are in tracking the discontinuities and in taking into account their interaction. Discontinuity tracking requires the development of reliable means for determining the location and time of the appearance of discontinuities. Multiple interactions between discontinuities are characterized by great diversity, but it can be reduced to several elementary interactions: collision of two counter propagating shock waves, absorption of a shock wave by an overtaking shock wave, and passage of a shock wave through a contact discontinuity.

2. MATHEMATICAL STATEMENT OF THE PROBLEM

We use the ideal gas approximation. Then, the problem is reduced to solving the system of gas-dynamic equations formed by the differential conservation laws for the mass, momentum, and energy supplemented with the proper initial and boundary conditions. Below, we present these equations in the Euler system of coordinates for the one-dimensional case:

$$\frac{\partial \rho}{\partial t} + \frac{\partial}{\partial x}(\rho u) = 0,$$

$$\frac{\partial}{\partial t}(\rho u) + \frac{\partial}{\partial x}(P + \rho u^2) = 0, \tag{2.1}$$

$$\frac{\partial}{\partial t}(\rho E) + \frac{\partial}{\partial x}(Pu + \rho u E) = 0, \text{ or } \frac{\partial}{\partial t}(\rho \mathscr{E}) + \frac{\partial}{\partial x}(\rho u \mathscr{E}) + P\frac{\partial u}{\partial x} = 0.$$

Here, $E = \mathscr{E} + \frac{u^2}{2}$, $P = \rho RT$, and $\mathscr{E} = \frac{R}{\gamma - 1} T$.

We use the notation ρ for the density, u for the velocity, P for the pressure, $\mathscr{E}$ for the internal energy, T for the temperature, R for the gas constant, and γ for the specific heat ratio.

Using the change of variables of the general type according to the dynamic adaptation method, we make the transformation to an arbitrary time-dependent system of coordinates with the variables (q, τ) in which Eqs. (2.1) are written as (see [19])

$$\frac{\partial}{\partial \tau}\left(\frac{\psi}{\rho}\right) + \frac{\partial}{\partial q}\left(\frac{Q}{\rho} - u\right) = 0,$$

$$\frac{\partial}{\partial \tau}(\psi u) + \frac{\partial}{\partial q}(P + Qu) = 0,$$

$$\frac{\partial}{\partial \tau}(\psi \mathscr{E}) + \frac{\partial}{\partial q}(Q\mathscr{E}) + P\frac{\partial u}{\partial q} = 0, \tag{2.2}$$

$$\frac{\partial \psi}{\partial \tau} = -\frac{\partial Q}{\partial q}, \quad \frac{\partial x}{\partial q} = \frac{\psi}{\rho},$$

where $\frac{\psi}{\rho}$ is the Jacobian of the transformation, Q is the transformation function (its physical meaning is the flux of matter through the boundary), and

$$\frac{\partial x}{\partial t} = -\frac{Q}{\rho} \tag{2.3}$$

is the velocity of the coordinate system.

As a result, we obtain an extended differential system (2.2) in the variables (q, τ), in which the last equation is the inverse transformation equation; in combination with the transformation Jacobian, it is used for determining the coordinates of the grid points, i.e., for the generation of the computational grid. The controlled distribution of the grid points for each time instant is performed using the transformation function Q, which is to be determined.

3. BREAKDOWN OF AN ARBITRARY DISCONTINUITY

The Riemann problem concerning the breakdown of an arbitrary discontinuity has been thoroughly studied. An analysis of its solution for the ideal gas can be found, for example, in [23, 47]. It is well known that the Riemann problem can appear in the simulation in two cases. First, when a discontinuity is present from the very beginning and it is required to consider the processes occurring after its breakdown. Second, any interaction of a shock wave with other shock waves and with contact discontinuities is reduced to the Riemann problem. As applied to the examination of processes in ideal gases, the following algorithm for determining the structure of the solution and of the gas-dynamic functions after an arbitrary discontinuity breakdown can be proposed.

Let the subscript $n = 1$ correspond to the parameters P_1, u_1, ρ_1, and T_1 on the left-hand side of the discontinuity and $n = 2$ correspond to the parameters P_2, u_2, ρ_2, and T_2 on its right-hand side. We want to find the parameters $P_3 = P_4$, $u_3 = u_4$, ρ_3, ρ_4, T_3, and T_4 after the breakdown, where (3–4) is the contact discontinuity that separates the gas in the state $n = 3$ (the left boundary of this portion of the gas is the wave (1–3)), and the gas in the state $n = 4$ (its right boundary is the wave (4–2)). It was shown in [23, 47] that, due to the self-similarity of the solution to the Riemann problem, the waves (1–3) and (2–4), if they exist, are either shock waves or rarefaction waves. Therefore, if $P_1 < P_3$, then (1–3) is a shock wave. In this case, the parameters P_3 and u_3 of state 3 belong to the Hugoniot adiabatic curve, which passes through the point (P_1, u_1). Otherwise, if $P_1 > P_3$, then (1–3) is a rarefaction wave. In this case, the parameters P_3 and u_3 of state 3 belong to the Poisson adiabat, which passes through the point (P_1, u_1). Similarly, the type of the wave (4–2) is determined, depending on relation between P_2 and P_4.

Using these facts, we define the function $F_n(P)$ for each of the states 1 and 2 of the discontinuity under examination (see [23]):

$$F_n(P) = \begin{cases} P_n + \dfrac{\gamma+1}{4}\left[\rho_n(u_3-u_n)^2 + \sqrt{\rho_n^2(u_3-u_n)^4 + \dfrac{16\gamma}{(\gamma+1)^2}P_n\rho_n(u_3-u_n)^2}\right], & P > P_n, \\ P_n\left[1 - \dfrac{\gamma-1}{2\sqrt{\gamma P_n/\rho_n}}(u_3-u_n)\right]^{\frac{2\gamma}{\gamma-1}}, & P < P_n. \end{cases}$$

In this definition, the first equation describes the Hugoniot adiabat, and the second one describes the Poisson adiabat. Equating $F_1(P)$ and $F_2(P)$, we use the Newton method to find the gas-dynamic velocity $u_3 = u_4$ on the contact discontinuity from the values P_1, u_1, ρ_1, P_2, u_2, and ρ_2 on the discontinuity. Upon finding $u_3 = u_4$, we determine $P_3 = P_4$, and then the other quantities: the densities ρ_3 and ρ_4, the temperatures T_3 and T_4, and (in the case of shock waves) the discontinuity velocities using the Hugoniot conditions

$$\begin{aligned} \rho_-(u_- - V) &= \rho_+(u_+ - V) = Q, \\ P_- + \rho_-(u_- - V)^2 &= P_+ + \rho_+(u_+ - V)^2, \\ \mathcal{E}_- + P_-/\rho_- + (u_- - V)^2/2 &= \mathcal{E}_+ + P_+/\rho_+ + (u_+ - V)^2/2. \end{aligned} \tag{3.1}$$

The subscripts (–) and (+) refer to the parameters on different sides of the discontinuity, and V and Q are the velocity and the flux of mass through the boundary.

Consider two situations:

(1) The left shock wave passes through the contact discontinuity or overtakes the right shock wave, which propagates in the same direction as the left wave.

(2) Two interacting counter propagating shock waves.

In the first case, the pressure satisfies the inequality $P_1 > P_3 = P_4 > P_2$, and the algorithm for continuing the calculations is as follows. On the left, a contact discontinuity is formed instead of the shock wave on which $u_3 = u_4$ and $P_3 = P_4$ are specified along with ρ_3 and T_3 on the left of the discontinuity and ρ_4 and T_4 on the right of it. The right boundary is replaced by the shock wave with P_4, u_4, ρ_4, and T_4 behind the front and P_2, u_2, ρ_2, and T_2 before the front. In the region between the discontinuities, the gas-dynamic quantities are assumed to be equal to P_4, u_4, ρ_4, and T_4. In the region to the left of the contact discontinuity, a rarefaction wave is propagating, which is not explicitly tracked.

In the second case, the pressure satisfies the inequalities $P_3 = P_4 > P_1$ and $P_3 = P_4 > P_2$, which somewhat complicates the calculation algorithm. On the left boundary, the shock propagating from the left to the right is replaced by a shock wave propagating in the opposite direction; its gas-dynamic parameters are P_3, u_3, ρ_3, and T_3 behind the front and P_1, u_1, ρ_1, and T_1 before the front. On the right, the shock wave is replaced by the contact discontinuity on which $u_3 = u_4$ and $P_3 = P_4$ are specified along with ρ_3 and T_3 on the left of the discontinuity and ρ_4 and T_4 on the right of it. Next, an auxiliary subregion with the left boundary coinciding with the contact discontinuity and the right-hand boundary coinciding with the shock wave with the parameters P_4, u_4, ρ_4, and T_4 behind the front and P_2, u_2, ρ_2, and T_2 before the front. In the region between the left shock wave and the contact discontinuity, all the gas-dynamic quantities are assumed to be equal to P_3, u_3, ρ_3, and T_3; between the contact discontinuity and the right shock wave, all the gas-dynamic quantities are assumed to be equal to P_4, u_4, ρ_4, and T_4.

4. BOUNDARY CONDITIONS

In the process of solution, different boundary conditions may be used in different calculation subdomains. For the problems considered in this paper, these conditions are classified as follows.

On the external steady boundaries, the impermeability condition is specified:

$$u = 0, \quad Q = 0. \tag{4.1}$$

On the left boundary, which corresponds to the piston(for the nonuniformly accelerating piston problem), the law of the piston motion is specified:

$$u = V(t), \quad Q = -\rho V(t). \tag{4.2}$$

On the external boundary that tracks the propagation of the perturbation over the background, the following boundary conditions are used:

$$u = 0, \quad \rho = \rho_0, \quad T = T_0, \quad Q = -\frac{\partial P}{\partial u}. \tag{4.3}$$

On the contact discontinuities, it holds that

$$u_+ = u_-, \quad P_- = P_+, \quad Q_- = Q_+ = 0. \tag{4.4}$$

Here, the subscripts (–) and (+) refer to the parameters on different sides of the discontinuity (to the left and to the right, respectively).

On the shock waves, Hugoniot condition (3.1) must be fulfilled. Since the three equations connect seven variables, four of them are determined by solving system (2.2) at the boundary points; these are the density, the velocity, and the temperature before the front of the shock wave and the velocity behind the front. The three other unknowns (the velocity of the discontinuity propagation and the density and the temperature behind the front of the shock wave) are determined from conditions (3.1). For example, when the shock wave propagates from the left to the right, conditions (3.1) yield V, ρ_-, and T_-.

This classification of the boundary conditions for the system of differential equations (2.2) completely closes the mathematical model under examination. The final form of the boundary conditions will be presented below for each particular problem.

5. FINITE DIFFERENCE APPROXIMATION

The numerical implementation of the model system of equations (2.1) in each of the subdomains of the computational space was performed on a grid with integer and half-integer grid points

$$\omega_{h,\Delta\tau} = \left\langle \begin{array}{c} (q_i, \tau^j), (q_{i+1/2}, \tau^j), q_{i+1} = q_i + h, q_{i+1/2} = q_i + 0.5h, i = 0, 1, \ldots, N-1 \\ \tau^{j+1} = \tau^j + \Delta\tau^j, j = 0, 1, \ldots \end{array} \right\rangle.$$

In the physical space, this grid is associated with the computational grid

$$\omega_{h,\Delta t} = \left\langle \begin{array}{c} (x_i^j, t^j), (x_{i+1/2}^j, t^j), x_{i+1}^j = x_i^j + h_{x,i}^j, x_{i+1/2}^j = x_i + 0.5h_{x,i}^j, i = 0, 1, \ldots, N-1 \\ h_{x,i}^j = h\left(\frac{\Psi}{\rho}\right)_{i+1/2}^j \\ t^{j+1} = t^j + \Delta t^j, j = 0, 1, \ldots \end{array} \right\rangle.$$

To approximate the differential equations, we used the finite difference method on staggered grids: the following family of difference schemes (see [19]) was set up in which the density $\rho_{i+1/2}$, the temperature $T_{i+1/2}$, the pressure $P_{i+1/2}$, and the internal energy $\mathscr{E}_{i+1/2}$ are determined at the half-integer points, and the velocity u_i and the function Q_i are determined at the integer points:

$$\frac{\Psi_{i+1/2}^{j+1} - \Psi_{i+1/2}^j}{\Delta\tau^j} = -\frac{Q_{i+1}^{\sigma_1} - Q_i^{\sigma_1}}{h_{i+1/2}},$$

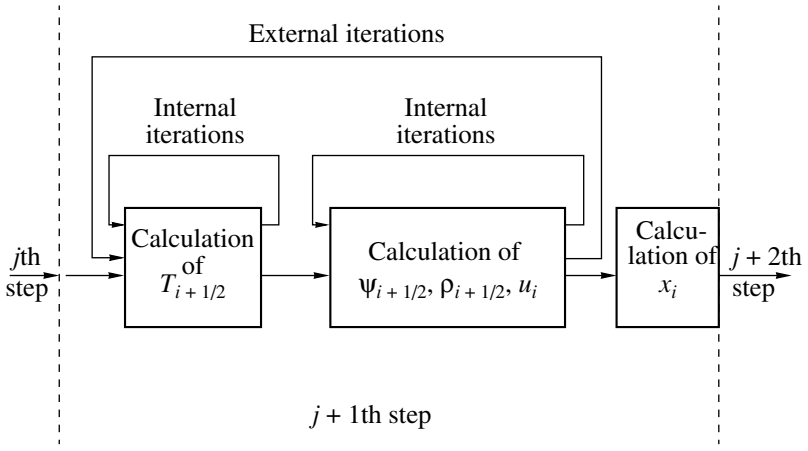

Fig. 1. Flowchart of the calculation algorithm.

$$\begin{aligned}
\frac{\psi_{i+1/2}^{j+1}/\rho_{i+1/2}^{j+1} - \psi_{i+1/2}^{j}/\rho_{i+1/2}^{j}}{\Delta\tau^j} &= -\frac{Q_{i+1}^{\sigma_1}/\rho_{i+1}^{\sigma_2} - Q_i^{\sigma_1}/\rho_i^{\sigma_2} - u_{i+1}^{\sigma_3} + u_i^{\sigma_3}}{h_{i+1/2}},\\
\frac{\psi_i^{j+1}u_i^{j+1} - \psi_i^j u_i^j}{\Delta\tau^j} &= -\frac{P_{i+1/2}^{\sigma_4} - P_{i-1/2}^{\sigma_4} + Q_{i+1/2}^{\sigma_1}u_{i+1/2}^{\sigma_3} - Q_{i-1/2}^{\sigma_1}u_{i-1/2}^{\sigma_3}}{0.5(h_{i+1/2}+h_{i-1/2})},\\
\frac{\psi_{i+1/2}^{j+1}\mathcal{E}_{i+1/2}^{j+1} - \psi_{i+1/2}^{j}\mathcal{E}_{i+1/2}^{j}}{\Delta\tau^j} &= -\frac{Q_{i+1}^{\sigma_1}\mathcal{E}_{i+1}^{\sigma_5} - Q_i^{\sigma_1}\mathcal{E}_i^{\sigma_5}}{h_{i+1/2}} - P_{i+1/2}^{\sigma_4}\frac{u_{i+1}^{\sigma_3} - u_i^{\sigma_3}}{h_{i+1/2}}.
\end{aligned} \tag{5.1}$$

Here, $f^{\sigma_r} = \sigma_r f^{j+1} + (1-\sigma_r)f^j$ and $\sigma_r = \sigma_1, \sigma_2, \ldots$ are the weight factors determining the degree to which the difference scheme is implicit. If $\sigma_1 = \sigma_2 = \ldots = 0$, then we obtain a completely explicit scheme with the approximation order $O(\Delta\tau + h^2)$. In the case $\sigma_1 = \sigma_2 = \ldots = 1$, the scheme is completely implicit and has the same order of approximation. In the case $\sigma_1 = \sigma_2 = \ldots = 0.5$, the order of approximation is $O(\Delta\tau^2 + h^2)$. The computations were performed using both the implicit scheme and the mixed scheme with the weight factors equal to 0.5. The computation results were almost independent of the weight factors; however, in the scheme with the second-order approximation with respect to time, the integration step was by a factor of 1.5–2 greater. In this paper, we present the results obtained using the completely implicit scheme of the first-order of approximation with respect to time and the second-order of approximation with respect to space.

For the functions $\{u, Q\} = f$ specified at the integer points of the grid ω, their values at the half-integer points were determined by the rule $f_{i+1/2} = 0.5(f_i + f_{i+1})$. Similarly, the values of the other functions $\{\psi, \rho, T, P, \mathcal{E}\} = f$ at the integer points were determined from the values of these functions at the half-integer points: $f_i = 0.5(f_{i-1/2} + f_{i+1/2})$.

An algorithm for solving Eqs. (5.1) is described in [19]. It is illustrated in Fig. 1. It involves two internal iteration blocks performed by the Newton method. The first iteration block solves the difference analog of the energy equation, and the second block solves the analogs of the equations of continuity, motion, and the equation governing the grid point redistribution (the first three equations in (5.1)). Both internal iteration blocks are included in the external iteration cycle. If the number of iteration steps in the external cycle exceeds seven or the number of iteration steps in the internal cycles exceeds ten, the time step is halved. If the number of iteration steps in the external cycle is less than four, then the next time step is increased 20%.

The initial value for all the unknown grid functions is determined by $f^{j+1^{(0)}} = f^j + (f^j - f^{j-1})\dfrac{\Delta\tau^j}{\Delta\tau^{j-1}}$.

The class of finite difference schemes used to solve the problems in this paper is classified as implicit schemes with central space differences; therefore, if the iteration process is convergent, these schemes are absolutely stable and converge to the solution with an accuracy determined by the order of approximation (see [23]). By the well-known Godunov theorem, there are no monotone schemes with an order of approximation with respect to space greater than one. Nevertheless, the use of higher order approximation schemes

is preferable to the use of the first-order schemes because they produce more accurate solutions on coarse grids in the case of smooth solutions. It is clear that the schemes proposed in this paper are not monotone because they have the second order of approximation with respect to space and use no monotonization techniques. However, the dynamic adaptation method helps explicitly track the greater part of the singularities in the solution (the shock waves and the contact discontinuities) thus eliminating the sources of nonmontonicity from the solution. Among the regions with high gradients, which can cause the violation of monotonicity, there remain only the rarefaction waves. The regions of the rarefaction waves expand with time thus decreasing the initial gradients of the unknown functions. This fact and the controlled motion of the grid points in the physical space that is coordinated with the unknown solution considerably reduce the appearing oscillations of the solution. Both these facts allow us to avoid tracking the boundaries of the rarefaction waves and avoid introducing monotonization procedures into the schemes for the problems under examination. We also stress that the use of the dynamic adaptation method does not contradict the use of various difference schemes and monotone algorithms (such as TVD or WENO) in a wide class of problems; it is rather an additional technique to those algorithms in the cases when it is desirable to redesign the computational grid near the singularities of the solution. However, this study shows that sometimes one can do without monotonization procedures. The main advantage of the dynamic adaptation method is that the grid point redistribution mechanism is introduced at the differential level (each of the initial equations includes the metric function ψ and the adaptation function Q related by the additional differential equation). It was shown in [13, 15] that the motion of the grid points coordinated with the solution considerably reduces the scheme variation.

6. SIMULATION RESULTS

1. The Woodward–Colella Problem

The Woodward–Colella problem describes the interaction of two counter propagating detonation waves that are formed as a result of the breakdown of two arbitrary discontinuities (see Figs. 2 and 3). From the mathematical point of view, this problem reduces to solving gas-dynamic equations (2.1) that include the differential conservation laws for the mass, momentum, and energy in the regions l, m, r: $x_l \in [0, 0.1)$, $x_m \in (0.1, 0.9)$, and $x_r \in (0.9, 1]$. At the initial moment, the gas with the specific heat ratio $\gamma = 1.4$ is in three different states in these three regions:

$$t = 0: \begin{pmatrix} \rho \\ u \\ P \end{pmatrix}_l = \begin{pmatrix} 1 \\ 0 \\ 10^3 \end{pmatrix}, \quad \begin{pmatrix} \rho \\ u \\ P \end{pmatrix}_m = \begin{pmatrix} 1 \\ 0 \\ 10^{-2} \end{pmatrix}, \quad \begin{pmatrix} \rho \\ u \\ P \end{pmatrix}_r = \begin{pmatrix} 1 \\ 0 \\ 10^2 \end{pmatrix}. \tag{6.1}$$

At the boundaries $x = 0$ and $x = 1$, the impermeability condition $u(t, 0) = u(t, 1) = 0$ is imposed. At the initial moment, two arbitrary discontinuities are placed at the points $x = 0.1$ and $x = 0.9$.

As a result of the breakdown of discontinuities (6.1) located at the points $x = \{0.1, 0.9\}$ (see Fig. 2), a complex structure is formed in the regions adjacent to these points. This structure includes rarefaction waves, contact discontinuites, and shock waves (Fig. 3). In order to determine this structure, the Riemann problem must be solved. We solve this problem using the algorithm described in Section 3, and obtain the structure depicted in Fig. 3. At the points of the initial discontinuities are the contact boundaries; from these boundaries, rarefaction waves are propagating towards the outer boundaries of the domain, and shock waves are propagating towards each other. Mathematically, this structure is described as follows:

$$t \approx 0: \begin{cases} x \in [0, 0.099], \quad \rho = 1, \quad u = 0, \quad P = 10^3, \\ x \in (0.099, 0.0995), \quad f(x) = f(0.099) + (x - 0.099)(f(0.0995) - f(0.099))/0.0005, \\ x \in [0.0995, 0.1), \quad \rho = 0.59, \quad u = 19.5976, \quad P = 460.9, \\ x \in (0.1, 0.101), \quad \rho = 5.99924, \quad u = 119.5976, \quad P = 460.9, \\ x \in [0.101, 0.899], \quad \rho = 1, \quad u = 0, \quad P = 10^{-2}, \\ x \in (0.899, 0.9), \quad \rho = 5.99242, \quad u = -6.1964, \quad P = 46.09, \\ x \in (0.9, 0.9005], \quad \rho = 0.583, \quad u = -6.1964, \quad P = 46.09, \\ x \in (0.9005, 0.901), \quad f(x) = f(0.9005) + (x - 0.9005)(f(0.901) - f(0.9005))/0.0005, \\ x \in [0.901, 1], \quad \rho = 1, \quad u = 0, \quad P = 10^2. \end{cases} \tag{6.2}$$

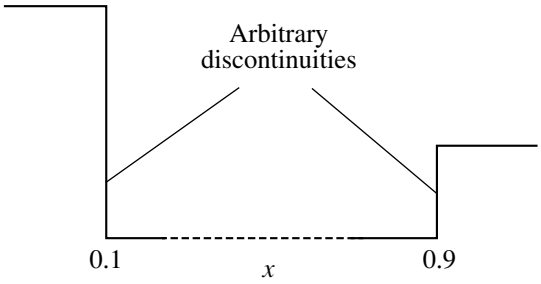

Fig. 2. A schematic profile of the pressure and temperature at the initial moment in the Woodward–Colella problem.

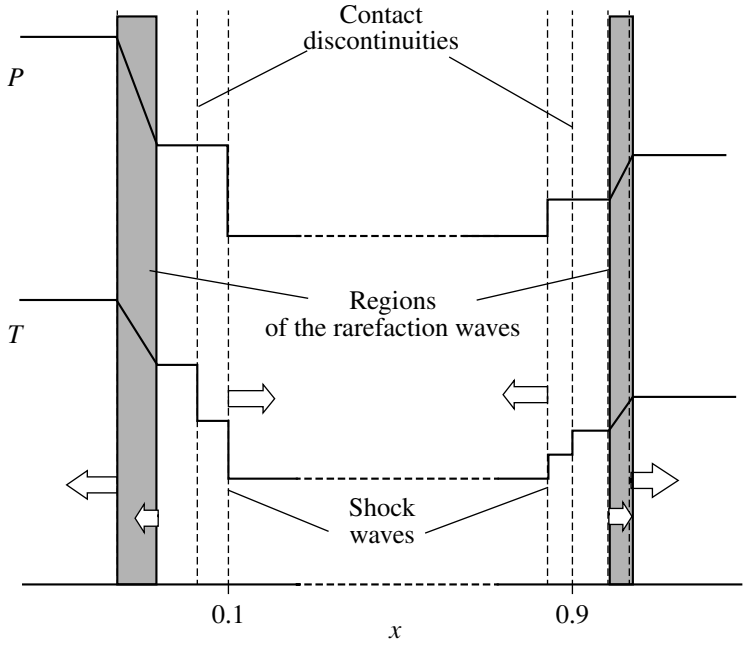

Fig. 3. Scheme of arbitrary discontinuity breakdown at the initial time (the profiles of the pressure P and the temperature T, the regions of the rarefaction waves are shaded); the arrows indicate the direction of the front propagation.

Here, $f(x)$ is any of the gas-dynamic functions ρ, u, and P determined by linear interpolation on x in the specified interval. At the initial time, it is assumed that $u_+ = u_-$ and $P_- = P_+$ at the boundaries $x = 0.1$ and $x = 0.9$. At $x = 0.101$ and $x = 0.899$ two shock waves satisfying Hugoniot conditions (3.1) are placed.

In terms of the variables (q, τ), the extended differential system (2.2), (2.3) must be complemented with the corresponding boundary and initial conditions. If we set $\psi = \rho$, then the Jacobian of the transformation is equal to unity. Therefore, the coordinates in the physical and in the computational space at the initial time coincide. Hence, initial conditions (6.2) written in terms of the variables (q, τ) do not change, and we do not repeat them here.

In the computational space, the boundaries $q = 0$ and $q = 1$ are immobile and impermeable (see (4.1)):

$$u(\tau, 0) = Q(\tau, 0) = 0, \quad u(\tau, 1) = Q(\tau, 1) = 0.$$

There is no flux of mass through the contact boundaries $q = 0.1$ and $q = 0.9$; therefore (see (4.4)), we have

$$u_-(\tau, 0.1) = u_+(\tau, 0.1), \quad P_-(\tau, 0.1) = P_+(\tau, 0.1), \quad Q(\tau, 0.1) = 0,$$

$$u_-(\tau, 0.9) = u_+(\tau, 0.9), \quad P_-(\tau, 0.9) = P_+(\tau, 0.9), \quad Q(\tau, 0.9) = 0.$$

The boundaries $q = 0.101$ and $q = 0.899$ are assumed to be moving and are explicitly tracked. Their velocity is determined from conservation laws (3.1).

In the evolution of the solution to the Riemann problem, several principal facts are distinguished.

1. The breakdown of two arbitrary discontinuities in the vicinity of the outer boundaries of the domain under consideration (see Fig. 2). As a result, at the points of the initial discontinuities contact boundaries are formed; from these boundaries, rarefaction waves are propagating towards the outer boundaries of the domain, and shock waves of different intensity are propagating towards each other (Fig. 3). A typical profile of the density is shown in Fig. 4.

2. The collision of the two shock waves results in the formation of a new contact discontinuity with two outgoing shock waves.

3. Passage of one of these shock waves through the contact discontinuity, which results in the formation of a rarefaction wave propagating in the opposite direction to the shock wave.

In the process of solution, the shock waves propagating towards each other collide, and this collision results in the formation of a contact discontinuity and two outgoing shock waves. This situation is also modeled by the Riemann problem with the parameters corresponding to the gas-dynamic characteristics behind the fronts of the shock waves. From the mathematical point of view, this collision results in the formation of an additional computational domain because we must track the appearing contact discontinuity (see item 3 above).

It has already been mentioned that in order to ensure the desired distribution of the grid points, the transformation function must depend on the unknown solution or on its features. The main feature of the solution of the problem of interacting counter propagating shock waves is the presence of moving discontinuities. The preliminary analysis shows that it is sufficient to use a quasi-uniform grid at each instant of time to solve this problem. A dynamic quasi-uniform distribution of the grid points can be obtained using one of the simplest forms of the function Q that is given by the so-called diffusive approximation [46, 48]

$$Q = -D\frac{\partial \psi}{\partial q}. \tag{6.3}$$

Here, D is the free parameter that has the meaning of the diffusion coefficient. Its value can be found from such parameters of the system as the geometric size of the domain and the velocity of the boundaries (see [48]). This value is found on the basis of a linear estimation of the size of the perturbation zone for the parabolic differential equations:

$$L \approx \sqrt{D\Delta t}.$$

In (6.3), D is chosen so as to ensure that the perturbation can cover the distance L equal to the distance between the moving boundaries in the time Δt. Representing Δt in terms of the velocity of the boundaries v as $\Delta t = \dfrac{\Delta L}{|v_l - v_r|}$, D can be written as $D = \dfrac{L^2|v_l - v_r|}{\Delta L}$, where $\Delta L = \dfrac{\psi}{\rho} L$ is the increment of the domain in time Δt and v_l and v_r are the velocities of the left and the right boundaries, respectively. Taking into account the expression for $v_{l,r} = -\left(\dfrac{Q}{\rho}\right)_{l,r}$, the coefficient D can be finally written as

$$D = \frac{|Q_l - Q_r|L}{\psi}.$$

In the discrete space of grid functions in which h is the space size and the length of the domain $L = hN$ is represented using the number of meshes N, D is written as

$$D = \frac{Nh|Q_l - Q_r|}{\psi_{\min}}. \tag{6.4}$$

Thus, the transformation function Q is related to the features of the problem under consideration; namely, with the domain size and the velocity of the boundaries $v_{l,r}$.

The processes in the Woodward–Colella problem were simulated taking into account the abovementioned initial and boundary conditions for system (2.2) and the particular form of the adaptation function Q (see (6.3), (6.4)).

Figures 5–12 show the spatial profiles of the velocity and density at various time instants found from the solution of the Woodward–Colella problem by the dynamic adaptation method with explicit discontinuity tracking. All these figures illustrate the solution obtained on the grid with the total number of grid points $N = 420$ containing 80 cells in each interior domain and 50 cells in each domain adjacent to the outer bound-

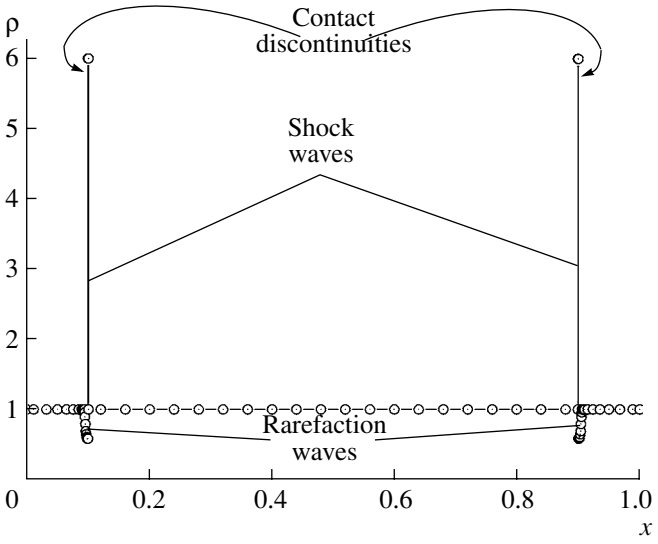

Fig. 4.

aries. Due to initial conditions (6.2), the evolution of each discontinuity has some specific features. In particular, the process as a whole is affected by the interaction of shock waves of various intensities. Figures 5 and 6 correspond to the time when the left rarefaction wave was already reflected from the outer boundary and approached the left shock wave while the right rarefaction wave only approached the opposite outer boundary ($t = 0.016$). The further propagation of the shock waves towards each other leads to still greater rarefaction in the regions between the shock waves and the outer boundaries.

The density and the velocity profiles at $t = 0.026$ immediately before the collision of the shock waves are shown in Figs. 7 and 8. In Figs. 9 and 10 at $t = 0.032$, they are shown immediately after the collision. The calculations were stopped when the right shock wave passed the right contact discontinuity (Figs. 11, 12) at $t = 0.038$. At that time, all the characteristic discontinuities are clearly visible: two shocks and three contact discontinuities. Note that the solutions obtained by various methods on the grids with less that 500 points give only a qualitative description of the behavior of gas-dynamic functions; the numerical values can be significantly inaccurate (for example, 10–50% for density). Figure 13 compares the density profiles obtained using the dynamic adaptation method and the modified WENO scheme [49]. It is seen that the dynamic adaptation method on a grid consisting of 420 cells produced almost the same solution (open dots) as WENO5m on 12 800 cells (solid line); the results obtained by WENO5m on a grid consisting of 400 cells are shown by diamonds.

2. Problem of a Nonuniformly Accelerating Piston

The problem concerning a nonuniformly accelerating piston can be obtained by modulating the law of motion of a uniformly accelerating piston by a periodic function of the type

$$u = V(t) = a_0 t + V_0[1 - \cos(\omega t)].$$

The statement of this problem is very close to the uniformly accelerating piston problem with the difference that the law of the piston motion has a periodic component in addition to the uniformly accelerating component. The periodic law of motion leads to the generation of a series of shock waves. They appear in the gas near the surface of the piston when it is accelerating and recede into the depth of the domain when it is decelerating. Since the piston law of motion includes an accelerating component, each next shock wave is more intensive than the previous one; when propagating, the next wave overtakes the previous one and absorbs it. At the place of absorption, a contact discontinuity is formed: a rarefaction wave is formed that propagates towards the piston, and a shock wave propagates in the opposite direction. Since the motion of the piston is periodic, the pattern of the gas-dynamic flow becomes more complicated with each new shock wave; this requires that the interaction of the shocks with the contact discontinuities be taken into account in addition to the interaction between the shock waves.

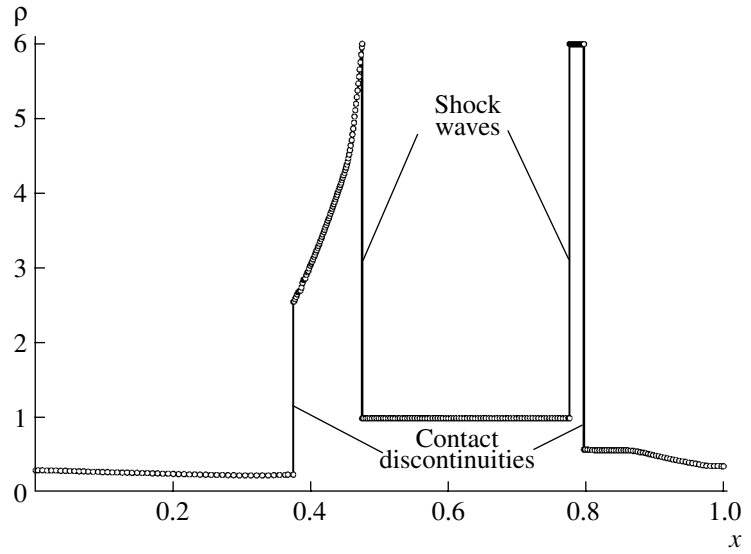

Fig. 5.

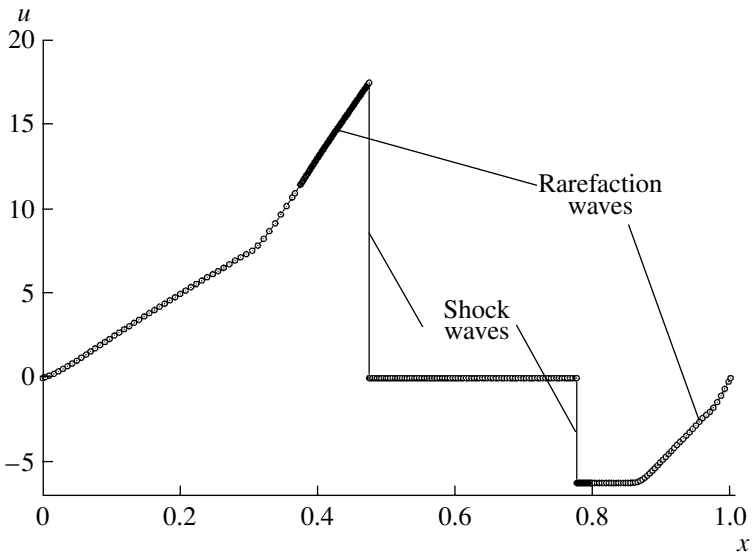

Fig. 6.

Application of the dynamic adaptation method to the nonuniformly accelerating piston problem is reduced to solving system of equations (2.2) with the corresponding initial and boundary conditions.

The initial conditions are as follows: $u = 0$, $P = P_0 = 1$ bar, $T = T_0 = 273°$K, and $\psi_0 = 1$.

The boundary conditions are as follows.

(a) On the piston

$u = V(t) = a_0 t + V_0[1 - \cos(\omega t)]$ (see (4.2)),

where $a_0 = 2.5 \times 10^{11}$ cm/s^2, $V_0 = 3 \times 10^4$ cm/s, $\omega = (\pi/2) \times 10^8$ 1/s.

(b) On the free boundary

$$u = 0,\ P = P_0,\ T = T_0,\ Q = -\frac{\partial P}{\partial u} \text{ (see (4.3)).}$$

The thermophysical characteristics are as follows: $C_v = 6.93 \times 10^{-1}$ J/g K and $R = 2.8668 \times 10^{-1}$ J/g K.

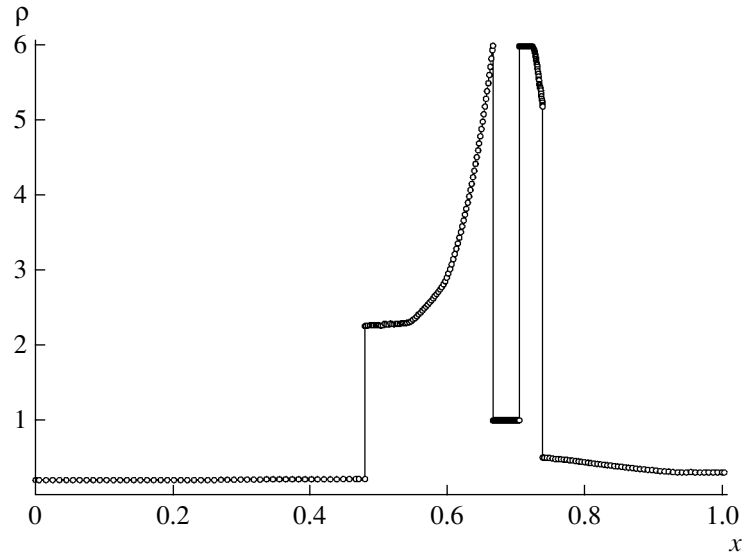

Fig. 7.

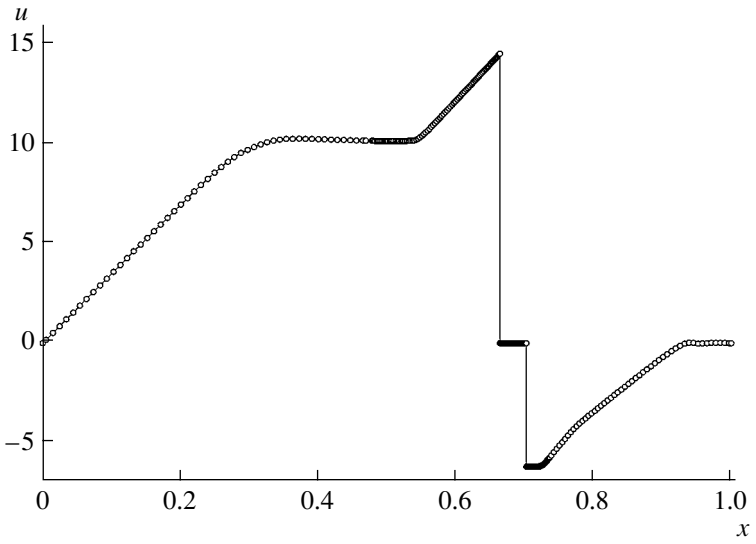

Fig. 8.

This problem was solved using a family of finite difference schemes written on staggered grids (see Section 5 and [19]). The modifications in the algorithm concerned only the mechanism of shock waves generation and interaction of discontinuities (shock–shock and shock–contact discontinuity).

When the inequality $u_{i-1} - u_{i+1} > \varepsilon$ (where ε is a small number) became true in each cell of the subdomain adjacent to the piston, the C_+ characteristics

$$C^j_{+,\,i-1/2} = 0.5(u_{i-1} + u_i) + \sqrt{\gamma R T_{i-1/2}},$$

$$C^j_{+,\,i+1/2} = 0.5(u_{i+1} + u_i) + \sqrt{\gamma R T_{i+1/2}}$$

were drawn from the centers of the cells $i - 1/2$ and $i + 1/2$. The time when these characteristics meet is found by the rule

$$t^j_c = (x_{i+1/2} - x_{i-1/2})/(C^j_{+,\,i-1/2} - C^j_{+,\,i+1/2}).$$

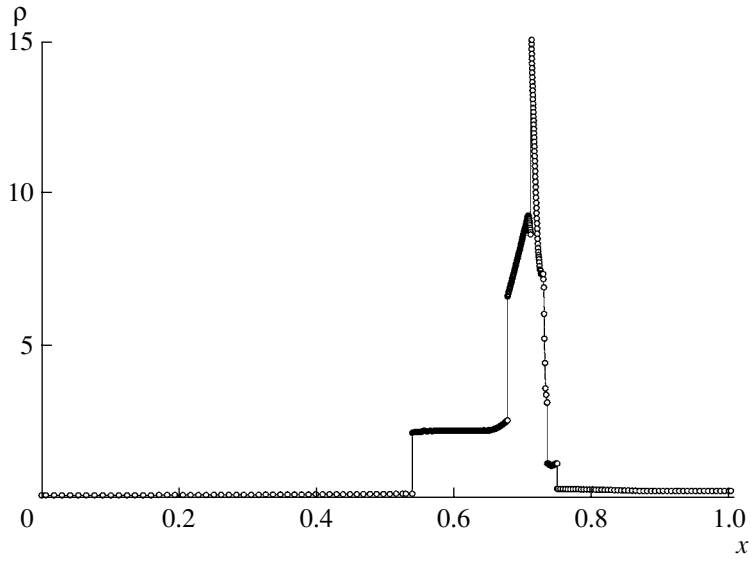

Fig. 9.

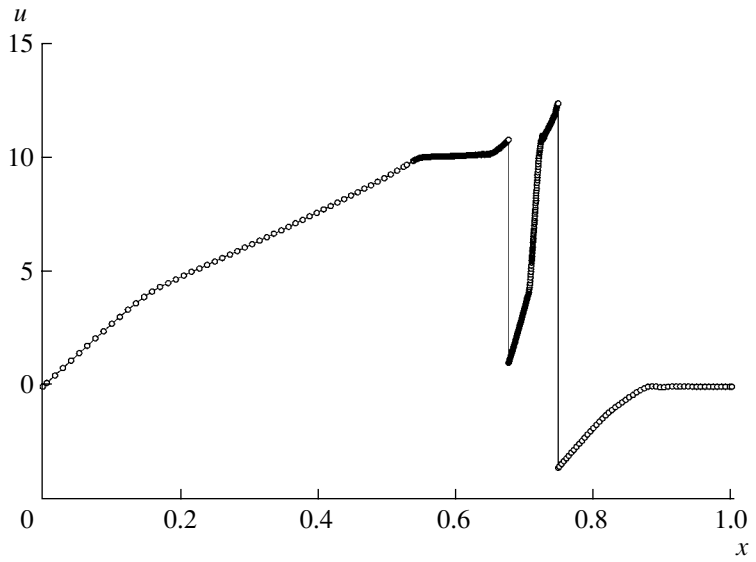

Fig. 10.

When $t^j + t_c^j$ attained its minimum and the coordinate of the intersection point fell in the computational subdomain, the time of the shock generation $t_{sw} = t + 0.95t_c$ was fixed, and the computation continued. The coefficient 0.95 is introduced to avoid violating the monotonicity of the gas-dynamic quantities caused by the excessive coarsening of space profiles. As soon as the time exceeded t_{sw}, a discontinuity was explicitly introduced on the left boundary of the cell with the maximal gradient. It was assumed that conservation laws (3.1) (Hugoniot conditions) were fulfilled on this discontinuity.

As in the Woodward–Colella problem, all the subsequent interactions between the discontinuities are reduced to the Riemann problem (see Section 3]). As a result, a contact discontinuity, and outgoing shock and rarefaction waves propagating in opposite directions are formed. Since the rarefaction waves are not explicitly tracked in the proposed algorithm, the number of tracked discontinuities before and after the interaction remains invariable. This allows one to make simple algorithmic modifications in the computation procedure for this case.

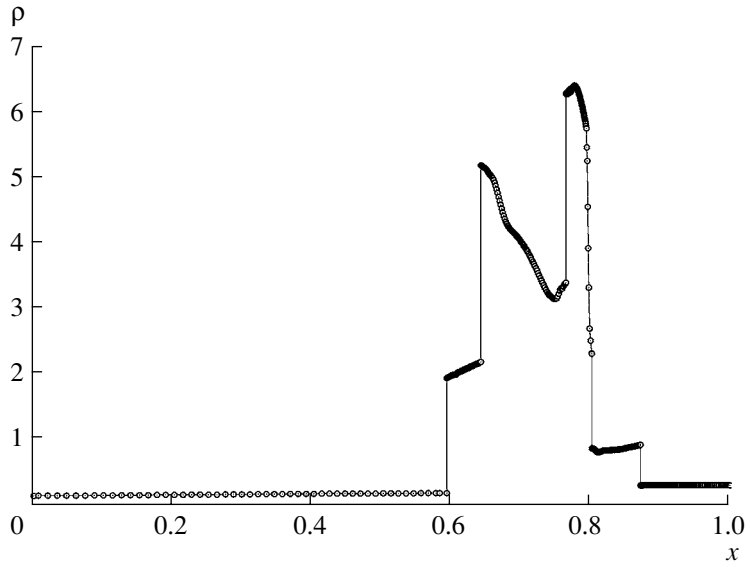

Fig. 11.

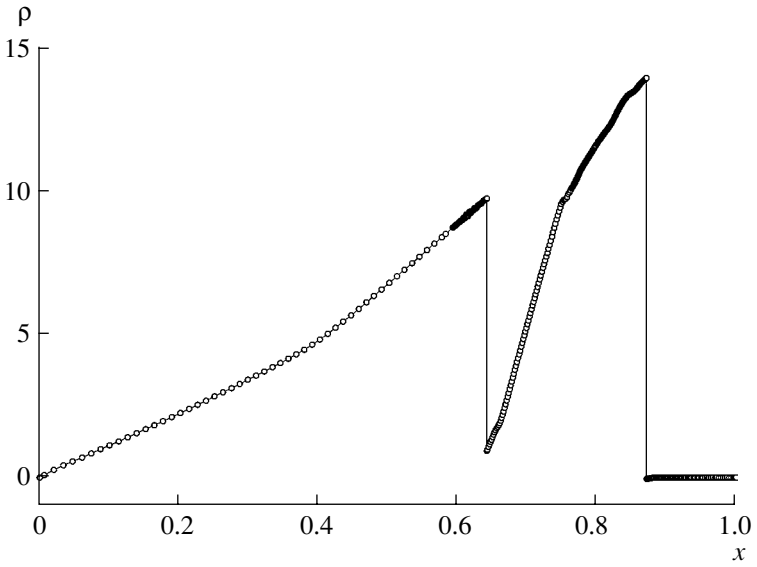

Fig. 12.

Choice of the transformation function *Q*. The main difficulties in the choice of the adaptation function Q in the problem of the interaction of the shock waves generated by the nonuniformly accelerating piston are caused by the requirement to use strongly nonuniform grids. The grid points in the domain adjacent to the piston must remain near the piston surface as long as possible because, due to the nonuniformity of the piston motion, the solution has high gradients here and shock waves are generated. The application of uniform grids is inefficient in this case because they have too many grid points. In the dynamic adaptation method, the distribution of the grid points is controlled by the choice of the function Q. To generate nonuniform grids, several types of functions Q can be used [4, 13, 19].

The diffusive approximation with the function $Q = -D\dfrac{\partial \psi}{\partial q}$ is attractive due to its simplicity. It was earlier used only for the generation of quasi-uniform grids [46, 48, 50]. However, if we reject the requirement for the propagation of the perturbation of ψ to the entire domain with moving boundaries and restrict ourselves to several grid cells, the diffusive approximation can be used for the generation of strongly nonuniform

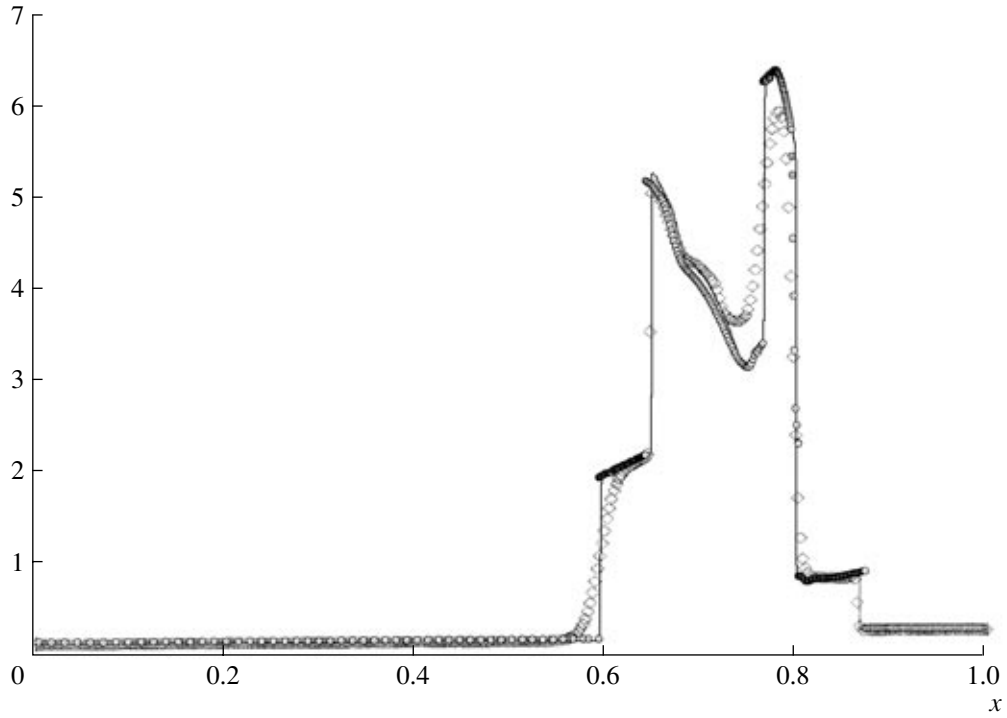

Fig. 13.

grids. The degree of nonuniformity depends on the size of the domain (or the number of cells) affected by the perturbation of ψ.

Using the derivation of the diffusion coefficient D in the Woodward–Colella problem and assuming that the perturbation affects only two intervals ($N = 2$), formula (6.4) can be modified as follows:

$$D = A(\psi)\frac{Nh|Q_l - Q_r|}{\psi_{\min}},$$

where $N = 2$ and $A(\psi) = \begin{cases} 1, & \psi \geq 1, \\ 1/\psi^2, & \psi < 1. \end{cases}$.

The factor $A(\psi) = \begin{cases} 1, & \psi \geq 1, \\ 1/\psi^2, & \psi < 1. \end{cases}$ is introduced to prevent two adjacent cells from collapsing when $\psi \ll 1$.

Simulation results. Simulation of the processes in the nonuniformly accelerating piston problem was performed with account for the initial and boundary conditions for system (2.2) formulated above and with account for the particular form of the adaptation function Q. The depth of the initial domain and the number of cells were $L = 3.2 \times 10^{-4}$ cm and $N = 380$.

Figures 14–16 show the space profiles of the gas-dynamic quantities and temperature at various time moments. In all the figures, the piston is located at $x = 0.0$ cm. At $t = 6 \times 10^{-8}$ s (Fig. 14), two shock waves are clearly visible; one of them was formed earlier and has already receded from the piston, and the other has just appeared. The latter wave has a large velocity and will finally absorb the former wave. At $t = 1.4 \times 10^{-7}$ s (Fig. 15), one wave has already absorbed the other, and two new shock waves appeared; one of them has passed through the contact discontinuity formed at the location of absorption. Finally, at $t = 1.8 \times 10^{-7}$ s (Fig. 16), three explicitly tracked shocks and two contact discontinuities are visible; i.e., by this time, the exterior shock was twice absorbed by the shocks formed later. Six space computational domains with one fixed and six explicitly tracked moving discontinuities are associated with these phenomena. Figure 17

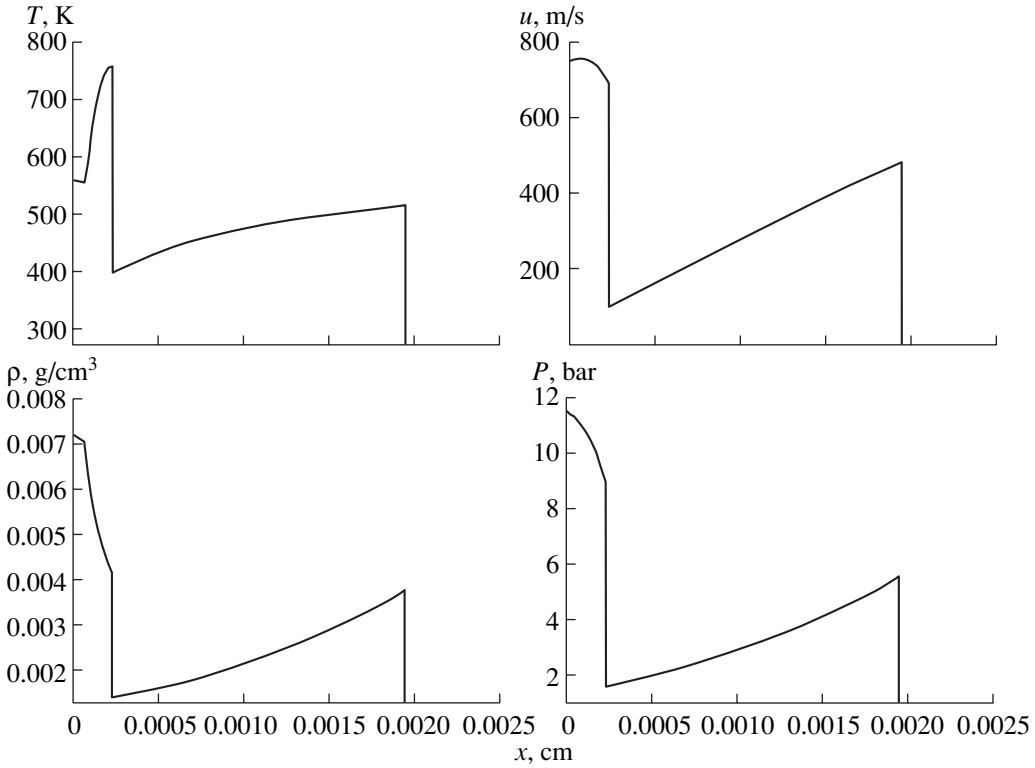
T, K
800
700
600
500
400
300
u, m/s
800
600
400
200
ρ, g/cm3
0.008
0.007
0.006
0.005
0.004
0.003
0.002
P, bar
12
10
8
6
4
2
0
0.0005
0.0010
0.0015
0.0020
0.0025
x, cm

Fig. 14.

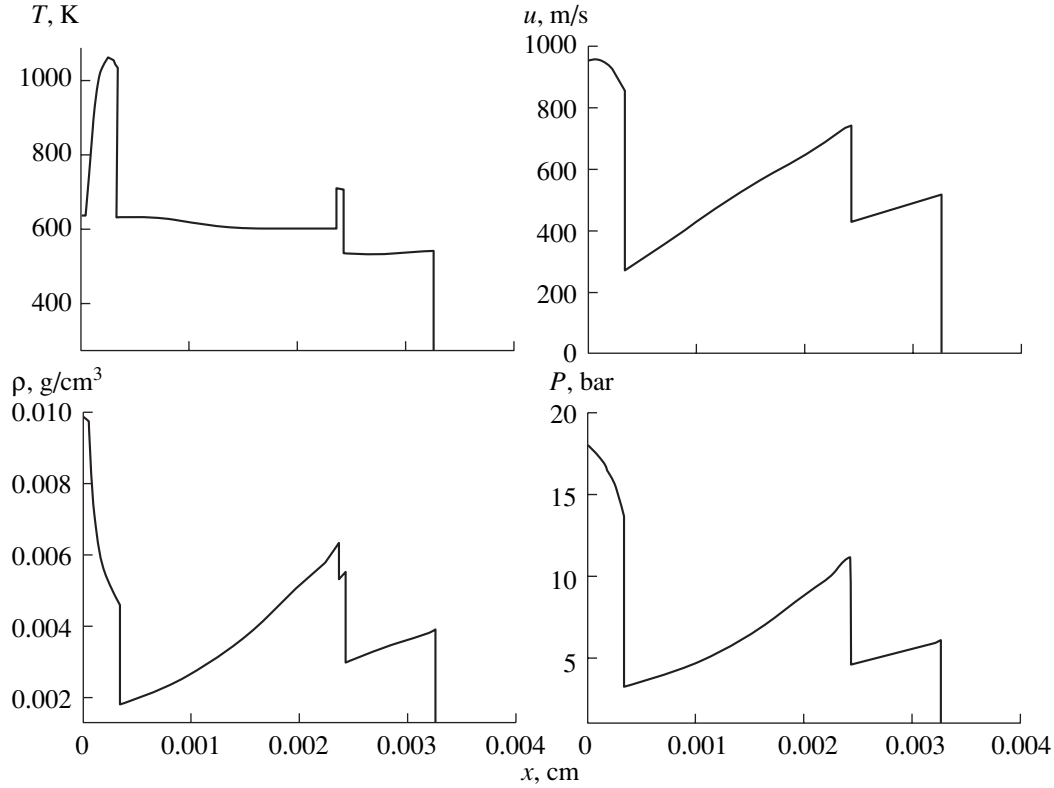
T, K
1000
800
600
400
u, m/s
1000
800
600
400
200
0
ρ, g/cm3
0.010
0.008
0.006
0.004
0.002
P, bar
20
15
10
5
0
0.001
0.002
0.003
0.004
x, cm

Fig. 15.

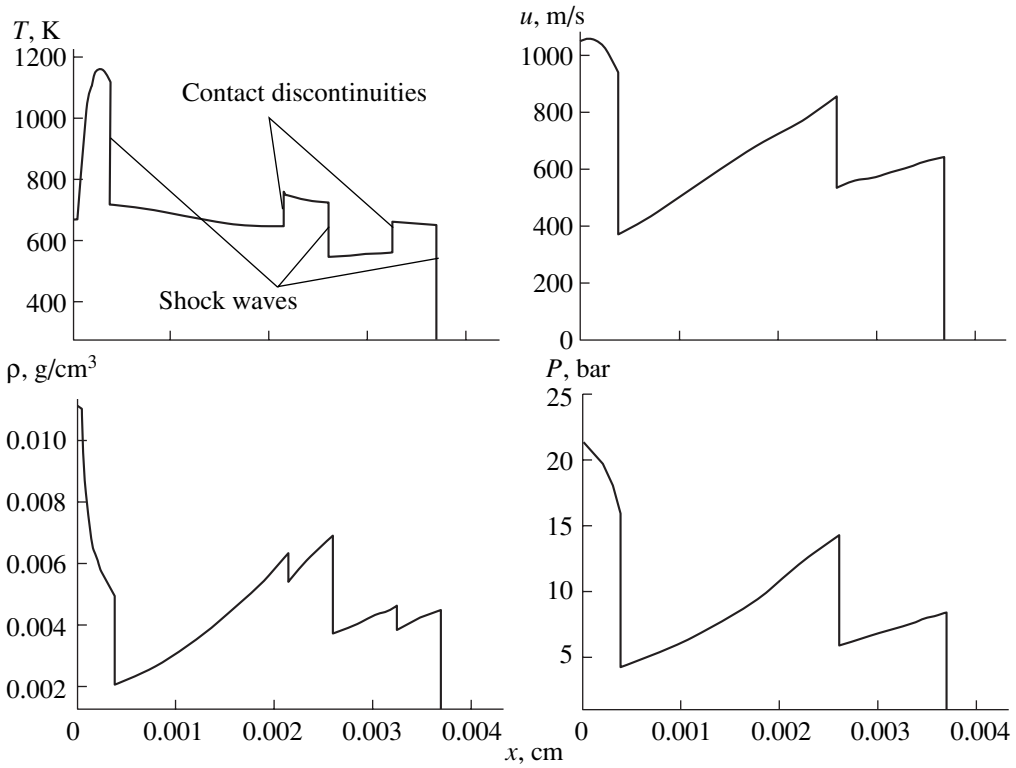

Fig. 16.

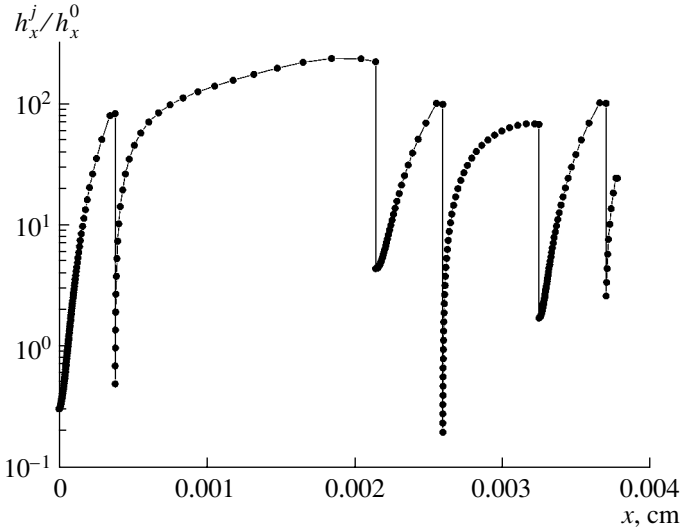

Fig. 17.

shows, at $t = 1.8 \times 10^{-7}$ s, the dependence $\frac{h_x^j}{h_x^0} = \left(\frac{\Psi}{\rho}\right)^j$ that describes the change of the size of the cells in the physical space by the end of the computation relative to their size at the initial moment. During computations, the ratio $\frac{h_x^j}{h_x^0}$ varied from 10^{-4} (before the interaction of the discontinuities) to 400 in various domains; i.e., the variation of the space grid size exceeded six orders of magnitude. This variation did not cause any complications in the computations.

7. CONCLUSIONS

The dynamic adaptation method as applied for gas dynamics problems with multiple interactions of discontinuities was considered. Using the test Woodward–Colella problem as an example, the efficiency of the proposed approach was demonstrated. The results obtained for the nonuniformly accelerating piston problem show that the dynamic adaptation method can be used in problems with multiple interactions of discontinuities when they are required to be explicitly tracked. For both problems, the diffusive adaptation function was used. This function made it possible, using a simple variation of the diffusion coefficients, to obtain results in each of these problems that are significantly different from the adaptation point of view. In the Woodward–Colella problem, where there is no need for mesh refinement in the vicinity of the singularities of the solution, the diffusion coefficient was chosen so as to generate a quasi-uniform grid in all the subdomains of the solution. In the nonuniformly accelerating piston problem, in contrast to the Woodward–Colella problem, there are two conflicting goals in the generation of the computational grid. On the one hand, at the initial stage of shock formation, the grid must be refined in the domain before the front. On the other hand, as the domain between the discontinuities shrinks, it is desirable to make the grid more and more uniform. A choice of the diffusion coefficient in the adaptation function was validated that makes it possible to satisfy both requirements by adapting the grid near the moving boundaries (which results in a strong nonuniformity of the grid in large subdomains of the solution) and by gradually making the grid size more uniform in the shrinking subdomains.

ACKNOWLEDGMENTS

This work was supported by the Russian Foundation for Basic Research, project nos. 04-01-00701 and 06-07-89191-a.

REFERENCES

1. J. F. Thompson, Z. U. Z. Warsi, and C. W. Mastin, *Numerical Grid Generation* (New York, North-Holland, 1985).
2. D. A. Anderson, "Equidistribution Schemes, Poisson Generators, and Adaptive Grid," Appl. Math. Comput. **24**, 211–227 (1987).
3. V. D. Liseikin, "Universal Elliptic Method for Adaptive Grid Generation," Zh. Vychisl. Mat. Mat. Fiz. **44**, 2167–2193 (2004) [Comput. Math. Math. Phys. **44**, 2062–2086 (2004)].
4. N. A. Dar'in and V. I. Mazhukin, "An Approach to Generation of Adaptive Grids," Dokl. Akad. Nauk SSSR **298**, 64–68 (1988).
5. D. A. Anderson, J. C. Tannehill, and R. H. Pletcher, *Computational Fluid Mechanics and Heat Transfer* (Hemisphere, New York, 1984; Mir, Moscow, 1990), Vols. 1, 2.
6. S. A. Ivanenko and G. P. Prokopov, "Methods of Adaptive Harmonic Grid Generation," Zh. Vychisl. Mat. Mat. Fiz. **37**, 643–662 (1997) [Comput. Math. Math. Phys. **37**, 627–645 (1997)].
7. *Applied Geometry, Grid Generation, and Highly Accurate Computations, Trudy Vserossiiskoi Konferentsii,* Ed. by Yu. G. Evtushenko, M. K. Kerimov, and V. A. Garanzha (Vychisl. Tsentr Ross. Akad. Nauk, Moscow, 2004) [in Russian].
8. M. J. Berger and P. Colella, "Local Adaptive Mesh Refinement for Shock Hydrodynamics," J. Comput. Phys. **82**, 64–84 (1989).
9. M. J. Berger, "Data Structures for Adaptive Grid Generation," SIAM J. Sci. Statist. Comput. **3**, 904–916 (1986).
10. J. M. Hyman and Sh. Li, *Iterative and Dynamic Control of Udaptive Mesh Refinement with Nested Hierarchical Grids*, Los Alamos Lab. Rep, No. 5462 (1998).
11. A. Andersen, X. Zheng, and V. Cristini, "Adaptive Unstructured Volume Remeshing. I: The Method," J. Comput. Phys. **208**, 616–625 (2005).
12. R. R. Nourgaliev, T. N. Dinh, and T. G. Theofanous, "Adaptive Characteristics-Based Matching for Compressible Multifluid Dynamics," J. Comput. Phys. **213**, 500–529 (2006).
13. V. I. Mazhukin, A. A. Samarskii, and A. V. Shapranov, "The Dynamic Adaptation Method in the Bürgers Problem," Dokl. Akad. Nauk **333**, 165–169 (1993).
14. V. D. Liseikin, "A Survey of Structured Adaptive Grid Generation Methods," Zh. Vychisl. Mat. Mat. Fiz. **36**, 3–41 (1996).
15. V. I. Mazhukin, O. Kastel'yanos, A. A. Samarskii, and A. V. Shapranov, "The Dynamic Adaptation Method in Nonstationary Problems with High Gradients," Mat. Modelir. **5** (4), 32–56 (1993).
16. N. A. Dar'in, V. I. Mazhukin, and A. A. Samarskii, "A Finite Difference Method for Solving One-Dimensional Gas Dynamics Problems on Adaptive Grids," Dokl. Akad. Nauk SSSR **302**, 1078–1081 (1988).

17. V. D. Liseikin, "Three-Dimensional Grid Generation Technique for Aerogasdynamics: A Survey," Vopr. Atom. Nauki Tekhn., Ser. Mat. Modelir. Fiz. Protsessov, No. 3, 31–45 (1991).
18. N. A. Dar'in, V. I. Mazhukin, and A. A. Samarskii, " A Finite Difference Method for Solving One-Dimensional Gas Dynamics Problems on Adaptive Grids that Are Dynamically Related to the Solution," Zh. Vychisl. Mat. Mat. Fiz. **28**, 1210–1225 (1988).
19. P. V. Breslavskii and V. I. Mazhukni, "The Dynamic Adaptation Method in Gas Dynamics," Mat. Modelir. **7** (12), 48–78 (1995).
20. A. N. Gil'manov, "Application of Dynamically Adaptive Grids to the Analysis of Flows with a Multiscale Structure," Zh. Vychisl. Mat. Mat. Fiz. **41**, 311–326 (2001) [Comput. Math. Math. Phys. **41**, 289–303 (2001)].
21. D. V. Rudenko and S. V. Utyuzhnikov, "Use of Dynamically Adaptive Grids for Modeling Three-Dimensional Unsteady Gas Flows with High Gradients," Zh. Vychisl. Mat. Mat. Fiz. **42**, 395–409 (2002) [Comput. Math. Math. Phys. **42**, 377–390 (2002)].
22. B. N. Azarenok, "A Scheme for Detonation Wave Computation on Moving Meshes," Zh. Vychisl. Mat. Mat. Fiz. **45**, 2260–2282 (2005) [Comput. Math. Math. Phys. **45**, 2174–2195 (2005)].
23. A. A. Samarskii and Yu. P. Popov, *Finite Difference Methods for Solving Gas Dynamics Problems*, 3rd ed. (Nauka, Moscow, 1992) [in Russian].
24. S. K. Godunov, A. V. Zabrodin, M. Ya. Ivanov, et al., *Numerical Solution of Multidimensional Gas Dynamics Problems* (Nauka, Moscow, 1976) [in Russian].
25. S. K. Godunov, "A Finite Difference Method for the Numerical Calculation of Discontinuous Solutions to Gas Dynamics Equations," Mat. Sb. **47** (3), 271–306 (1959).
26. B. Van Leer, "Towards the Ultimate Conservative Finite Difference Scheme. I. The Quest of Monotonicity," Lect. Notes Phys. **18** (1), 163–168 (1973).
27. B. Van Leer, "Towards the Ultimate Conservative Finite Difference Scheme. II. Monotonicity and Conservation Combined in a Second Order Scheme," J. Comput. Phys. **14** (4), 361–376 (1974).
28. J. P. Boris, D. L. Book, and K. Hain, "Flux-Corrected Transport. II. Generalization of the Method," J. Comput. Phys. **18**, 248–283 (1975).
29. J. P. Boris and D. L. Book, "Flux-Corrected Transport. III Minimal-Error FCT Algorithms," J. Comput. Phys. **20**, 397–431 (1976).
30. E. S. Oran and J. P. Boris, *Numerical Simulation of Reactive Flow* (Elsevier, New York, 1987; Mir, Moscow, 1990).
31. A. Harten, "High Resolution Schemes for Hyperbolic Conservation Laws," J. Comput. Phys. **49**, 357–393 (1983).
32. A. Harten, "On a Class of High Resolution Total-Variation-Stable Finite-Difference Schemes," SIAM J. Numer. Anal. **21**, 1–23 (1984).
33. S. Osher, "Riemann Solvers, the Entropy Condition, and Difference Approximation," SIAM J. Numer. Anal. **21**, 217–235 (1984).
34. S. Osher and C.-W. Shu, "Efficient Implementation of Essentially Non-Oscillatory Shock-Capturing Schemes," J. Comput. Phys. **77**, 439–471 (1988).
35. A. Harten, "ENO Schemes with Subcell Resolution," J. Comput. Phys. **83**, 148–184 (1989).
36. X.-D. Liu, S. Osher, and T. Chan, "Weighted Essentially Non-Oscillatory Schemes," J. Comput. Phys. **115**, 200–212 (1994).
37. Ph. Colella and P. R. Woodward, "The Piecewise Parabolic Method (PPM) for Gas-Dynamical Simulations," J. Comput. Phys. **54**, 174–201 (1984).
38. A. G. Kulikovskii, N. V. Pogorelov, and A. Yu. Semenov, *Mathematical Issues in the Numerical Solution of Hyperbolic Equations* (Fizmatlit, Moscow, 2001) [in Russian].
39. Yu. A. Bondarenko, V. V. Bashurov, and Yu. V. Yanilkin, *Mathematical Models and Numerical Methods for Unsteady Gas Dynamics Problems: A Survey*, Preprint, No. 88, RFYaTs-VNIIEF (2003).
40. R. J. LeVeque and K. M. Shyue, "One-Dimensional Front Tracking Based on High Resolution Wave Propagation Methods," SISC **16**, 348–377 (1995).
41. B. Van Leer, "Towards the Ultimate Conservative Difference Scheme. V. A Second Order Sequel to Godunov's Method," J. Comput. Phys. **32**, 101–136 (1979).
42. W. D. Henshaw, "A Scheme for Numerical Solution of Hyperbolic Systems of Conservation Laws," J. Comput. Phys. **68**, 25–47 (1987).
43. K. M. Shyue, "An Efficient Shock-Capturing Algorithm for Compressible Multicomponent Problems," J. Comput. Phys. **142**, 208–242 (1998).
44. S. A. Ivanenko and A. A. Charakhch'yan, "Curved Grids Consisting of Convex Quadrangles," Zh. Vychisl. Mat. Mat. Fiz. **28**, 503–514 (1988).

45. V. D. Liseikin, "On Some Interpretations of a Smoothness Functional Used in Constructing Regular and Adaptive Grids," Russ. J. Numer. Anal. Modell. **8**, C. 507–518 (1993).
46. P. V. Breslavskii and V. I. Mazhukin, "Mathematical Modeling of Pulse Melting and Evaporation of Metals with the Explicit Tracking of the Interphase Boundaries," Inzh.–Fiz. Zhurnal **57** (1), 107–114 (1989).
47. L. V. Ovsyannikov, *Lectures in the Foundations of Gas Dynamis* (Izhevsk, Institut Komputernykh Issledovanii, 2003) [in Russian].
48. O. N. Koroleva and V. I. Mazhukin, "Mathematical Simulation of Laser Induced Melting and Evaporation of Multilayer Materials," Zh. Vychisl. Mat. Mat. Fiz. **46**, 887–901 (2006) [Comput. Math. Math. Phys. **46**, 848–862 (2006)].
49. A. K. Henrick, T. D. Aslam, and J. M. Powers, "Mapped Weighted Essentially Non-Oscillatory Schemes: Achieving Optimal Order Near Critical Points," J. Comput. Phys. **207**, 542–567 (2005).
50. V. I. Mazhukin, I. Smurov, C. Dupuy, and D. Jeandel, "Simulationn of Laser Induced Melting and Evaporation Processes in Superconducting Ceramics," J. Numer. Heat Transfer **26** Part A, 587–600 (1994).